2014

Hydrodynamic-Pressure-Induced Elastic Deformation of Thrust Slide-Bearings in Scroll Compressors and Oil Film Pressure Increase Due to Oil Envelopment

Noriaki Ishii
Osaka Electro-Communication University, Japan, ishii@isc.osakac.ac.jp

Takuma Tsuji
Mayekawa MFG. Co., Ltd., takuma-tsuji@mayekawa.co.jp

Keiko Anami
Ashikaga Institute of T, k.anami@nifty.com

Charles W. Knisely
Bucknell University, US, knisely@bucknell.edu

Tatsuya Oku
Mayekawa MFG. Co., Ltd., tatsuya-oku@mayekawa.co.jp

See next page for additional authors

Authors
Noriaki Ishii, Takuma Tsuji, Keiko Anami, Charles W. Knisely, Tatsuya Oku, Koichi Nokiyama, Kiyoshi Sawai, Hirofumi Yoshida, and Hiroaki Nakai

Hydrodynamic-Pressure-Induced Elastic Deformation of Thrust Slide-Bearings in Scroll Compressors and Oil Film Pressure Increase Due to Oil Envelopment

Noriaki ISHII[1]*, Takuma TSUJI[2], Keiko ANAMI[3], Charles W. KNISELY[4], Tatsuya OKU[2], Koichi NOKIYAMA[1], Kiyoshi SAWAI[5], Hirofumi YOSHIDA[6] and Hiroaki NAKAI[6]

[1] Osaka Electro-Communication Univ., Dept. of Mechanical Engineering, Osaka, Japan.
Tel/fax: +81-72-820-4561, E-mail: ishii@isc.osakac.ac.jp
[2] Research and Development Center, Mayekawa MFG. Co., Ltd., Ibaraki, Japan,
E-mail: tatsuya-oku@mayekawa.co.jp
[3] Ashikaga Institute of Technology, Dept. of Mechanical Engineering, Tochigi, Japan.
E-mail: anami@ashitech.ac.jp
[4] Bucknell Univ., Dept. of Mechanical Engineering, Lewisburg, Pennsylvania, USA.
E-mail: knisely@bucknell.edu
[5] Dept. of Mechanical Engineering, Hiroshima Institute of Technology, Hiroshima, Japan.
E-mail: sawai@me.it-hiroshima.ac.jp
[6] Air-Conditioning and Cold Chain Development Center, Corporate Engineering Division Appliances Company, Panasonic Corporation, Shiga, Japan.
E-mail: yoshida.hirofumi@jp.panasonic.com

ABSTRACT

In this paper, the effect of the Elasto-Hydrodynamic Lubrication (EHL) on the performance of thrust slide-bearings in scroll compressors is considered. The EHL effect accounts for the superior lubrication characteristics of these bearings. The orbiting thrust plate undergoes elastic deformation due to axial loading, resulting in the formation of a uniform fluid wedge between the orbiting and fixed thrust plates. This fluid wedge is a region with very high induced oil film pressure which, in turn, accounts for the remarkably good lubrication characteristics of the thrust slide-bearing. Furthermore, the high oil film pressure further induces a local elastic deformation of the fixed thrust plate to form an EHL pocket in the thrust plate. The greater the deformation, the more the oil film pressure between the sliding surfaces increases, due to the envelopment of the oil in this local region of deformation. The formation of the EHL pocket was verified using FEM analysis and lubrication tests on the elastic deformation of the thrust plate.

Key Words : Lubrication, Tribology, EHL, Soft EHL, Thrust Slide-Bearing, Scroll Compressor, Refrigerant

1. INTRODUCTION

The scroll compressor is a low-vibration and low-noise high-performance compressor that compresses refrigerant by the use of crescent-shaped multiple compression chambers formed by two pairs of spiral walls of the orbiting and fixed scrolls. Scroll compressors are extensively used in heat pump and air-conditioning applications. Figure 1 shows a cross-sectional view of the compression mechanism of a scroll compressor. Figure 1(a) shows an overall view and Figure 1(b) an enlarged view of the compression mechanism. The lubrication mechanism of the thrust slide bearing of scroll compressor has not yet been definitively elucidated. Recently, however, detailed characterization of the lubrication mechanism has been provided by both experimental and theoretical studies (see Ishii, *et al.* (2008) and Oku, *et al.* (2008)). It was suggested that the elasto-hydrodynamic lubrication (EHL) effect and the envelopment of lubricating oil into EHL pockets on the faces of the orbiting and fixed thrust plates in the thrust slide bearing of a scroll compressor leads to its superior lubrication performance.
In general, elasto-hydrodynamic lubrication (EHL) is understood as a “phenomenon that brings about satisfactory lubricating conditions as the local contact portion makes an elastic deformation on the gear tooth

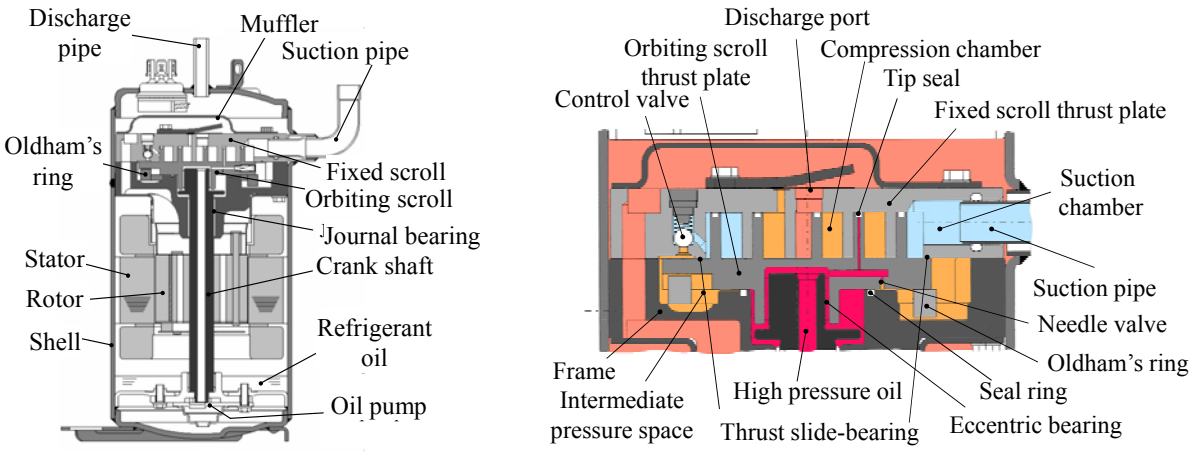

(a) Cross sectional view (b) Compression mechanism

Figure 1 : High pressure type scroll compressor.

contact surface, etc. and in that portion, oil is confined and acquires ultrahigh pressure." In the thrust slide bearing of scroll compressors, such isolated local contact points do not occur, but the thrust plate undergoes macroscopic elastic deformation due to oil film pressure. The resulting elastic deformation is postulated to give rise to the EHL effect in thrust slide bearings, thereby increasing lubrication performance.

In the present study, an analysis of the fluid lubrication of thrust slide bearing as a mixed lubrication process is presented using the average Reynolds equation of Patir & Cheng (1978 ; 1979) along with the solid contact theory from Greenwood & Williamson. The analysis will specifically addresses the EHL effect in thrust slide bearings, termed **soft EHL**, since it is more dispersed than the EHL previously identified in the lubrication of gear teeth. Further, the analysis does not consider the compressibility of the lubricant nor any changes in its viscosity. The soft EHL presented herein assumes constant lubricant density and viscosity. Subsequently, the elastic deformation of the thrust plate by high oil-film pressure is considered and is shown to give rise to the envelopment of the lubricating oil. Lastly, the formation of pocket-shaped elastic deformations is verified both through experiments on and by FEM analysis of a small-size scroll compressor thrust bearing by Tsuji (2014).

2. OUTLINE OF LUBRICATION THEORY ANALYSIS OF THRUST SLIDE BEARING AND SOFT EHL ANALYSIS

The lubrication of thrust slide bearing was theoretically analyzed by Oku, *et al.* (2008). In this section, an outline of their theoretical analysis is presented. The conditions under which the elastic deformation of the thrust plate forms a wedge angle relative around its outer circumference are represented by a theoretical of the rigid body thrust plate, as shown in upper portion of Figure 2. In order to enable the measurement of the friction force working on the orbiting scroll thrust plate shown in Figure 1, the orbiting scroll thrust plate in the model is immobilized, positioned, and supported in the horizontal plane by a pivot bearing positioned on its upper surface. In this manner, the degree of freedom of the thrust plate rotating around the pivot bearing is maintained. Furthermore, since the pivot shaft is allowed to move in the thrust direction, the thrust plate has a degree of freedom in the vertical direction. The orbiting scroll thrust plate in the actual compressor, shown in Figure 1, is loaded by a pressure difference and it deforms, producing a

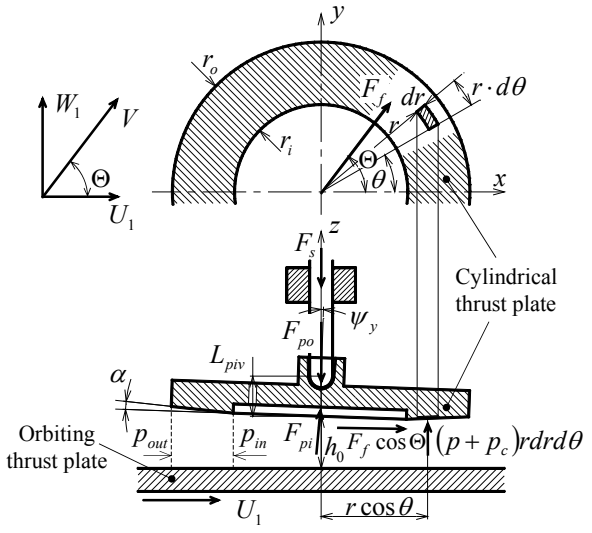

Figure 2 : Mathematical model of rigid thrust slide-bearing with a forced wedge at its periphery, for theoretical analysis of fluid lubrication.

wedge angle around its outer periphery. In the thrust plate model (in Figure 2), the bottom surface of the now fixed equivalent of the orbiting thrust plate is inclined at an angle of α to provide a geometry relative similar to the elastically deformed orbiting thrust plate. The fixed scroll thrust plate, shown on the top in Figure 1, is located on the lower side of the model and is powered by a motor to undergo an orbiting motion. In this manner, the same relative motion is obtained (for further detail, see Ishii *et al*. (2008) and Oku, *et al*. (2008)). In the model (Figure 2), a large gas force F_{po} acts downward on the top surface of the cylindrical thrust plate (now fixed) and a small gas force F_{pi} acts upward on its bottom surface. Due to this difference in pressure loading, the cylindrical thrust plate is pressed against the now orbiting scroll thrust plate. To enable experiments with no gas force difference, a downward acting spring thrust load F_s is applied to the fixed scroll thrust plate to press it downward. The pivot bearing is located at the center of the fixed scroll thrust plate. The two radii, r_i and r_o denote the inner and outer radial, respectively, of the annular region of the thrust slide bearing where the fixed cylindrical thrust plate is pressed against the orbiting scroll thrust plate. The fixed scroll thrust plate can rotate around both the *x*-axis and the *y*-axis. The symbols ψ_x and ψ_y denote the rotation angles around *x*-axis and *y*-axis of the fixed scroll thrust plate, respectively. An oil film is confined between the fixed scroll thrust plate and the orbiting scroll thrust plate (now on the lower side). The two pressures, p_{out} and p_{in}, denote the boundary pressure on the outer and inner circumferences. The boundary velocity of the oil film is given by the velocity *V,* which corresponds to the thrust plate velocity as it undergoes orbital motion. The angle Θ denotes the direction of *V* from the *x*-axis. The total frictional force F_f works in that direction. The symbols U_1 and W_1 denote the *x* and *y*-components of *V*.

2.1 Oil Film Pressure and Oil-Film Force

Expressing the oil film thickness *h* in polar coordinates (r, θ) with its origin at the bearing center *O*, we have

$$h(r,\theta) = h_0 + (r - r_i)\tan\alpha - r\cos\theta\cdot\psi_y + r\sin\theta\cdot\psi_x + \delta(r,\theta;t) \quad \left(r_i < r < r_o\right) \tag{1}$$

where h_o denotes the average clearance height and δ the elastic deformation rate. Assuming that the oil can be treated as an isothermal incompressible fluid, the oil-film pressure *p* that acts on the rough bearing surface can be computed using Equation (2) below, with the average Reynolds expression derived by Patir & Cheng (1978 ; 1979) written in polar coordinates.

$$\begin{aligned}\frac{1}{R}\frac{\partial}{\partial R}\left(\varphi RH^3\frac{\partial P}{\partial R}\right)+\frac{1}{R^2}\frac{\partial}{\partial\theta}\left(\varphi H^3\frac{\partial P}{\partial\theta}\right) &= \lambda\cdot\frac{1}{R}\left\{\frac{\partial}{\partial R}\left(\overline{H}_T\cos(\theta-\Theta)\right)-\frac{\partial}{\partial\theta}\left(\overline{H}_T\sin(\theta-\Theta)\right)\right\}\\ &+\lambda\sigma\frac{1}{R}\left\{\frac{\partial}{\partial R}\left(\varphi_s R\cos(\theta-\Theta)\right)-\frac{\partial}{\partial\theta}\left(\varphi_s\sin(\theta-\Theta)\right)\right\}+\sigma_s\frac{\partial\overline{H}_T}{\partial\tau_t}\end{aligned} \tag{2}$$

where the non-dimensional variables are defined by the following equations have been introduced.

$$R \equiv r/r_o\ ,\quad P \equiv p/p_a\ ,\quad H \equiv h/h_{ref}\ ,\quad \overline{H}_T \equiv \overline{h}_T/h_{ref}\ ,\quad \tau_t \equiv \omega t \tag{3}$$

where p_a denotes atmospheric pressure and h_{ref} an arbitrary standard oil film thickness in the thrust slide bearing, assumed to be 10 μm, as a typical value. $\overline{h}_T$ represents the average oil film thickness which can be obtained by integrating the local film thickness h_T. ω denotes the orbiting velocity of the orbiting scroll thrust plate (lower side) and *t* is time. σ denotes the standard deviation of surface roughness of the composite top and bottom surfaces ($=\sqrt{\sigma_1^{\,2}+\sigma_2^{\,2}}$). σ_1 and σ_2 are standard deviations of the respective asperity heights of the orbiting scroll thrust plate and the fixed scroll thrust plate. λ in Equation (2) denotes the number of bearings and σ_s the squeeze number, which are defined as follows:

$$\lambda \equiv \frac{6\mu^* V}{r_o p_a}\left(\frac{r_o}{h_{ref}}\right)^2\ ,\quad \sigma_s \equiv \frac{12\mu^*\omega}{p_a}\left(\frac{r_o}{h_{ref}}\right)^2 \tag{4}$$

where, μ^* denotes the viscosity of lubricating oil. The symbols φ and φ_s denote the pressure-flow coefficient and shear-flow coefficient, respectively. In this model, the thrust plate is assumed to have isotropic roughness.

The oil-film pressure generated on the bearing surface can be found by solving the average Reynolds equation under the boundary conditions. Integrating the oil-film pressure over the whole bearing surface gives the oil-film force F_{OIL} as follows:

$$F_{OIL} = \iint p(r,\theta)\, r d\theta dr \tag{5}$$

The viscous resistance force F_{VS} that works on the bearing surface can be calculated by the following equation with the surface roughness taken into account:

$$F_{vs} = \iint \frac{\mu^* V}{h}\left[\left(\phi_f + \phi_{fs}\right) - 2V_{r2}\phi_{fs}\right] r d\theta d\theta \tag{6}$$

where ϕ_f and ϕ_{fs} denote shear stress coefficients and V_{r2} denotes the fractional deviation of roughness.

2.2 Solid Contact Force and Solid Frictional Force

According to the solid contact theory of Greenwood & Williamson (1966), the local solid contact ratio $\alpha^*(r, \theta)$ is given by the following equation:

$$\alpha^*(r,\theta)\left(\equiv \frac{dA}{r d\theta dr}\right) = \pi\eta\beta\sigma\int_{H_r}^{\infty}(s - H_r)\phi^*(s)ds \tag{7}$$

$\phi^*(s)$ represents a distribution function of asperity summit height normalized by the standard deviation of asperity summit height, whereas β denotes the asperity tip curvature radius. H_r is defined by the ratio of apparent clearance (h-1.1σ) to the standard deviation $\sigma^*(= 0.7\sigma)$ of asperity summit height in the Greenwood-Williamson model and is given by the following equation:

$$H_r = \frac{h - 1.1\sigma}{\sigma^*} \tag{8}$$

If Equation (7) is used, the solid contact force F_{sc} and the solid frictional force F_{ss} can be found by the following equation:

$$F_{sc}\left(\equiv \int p_c \cdot dA\right) = \int\int p_c \alpha^*(r,\theta)\cdot r d\theta dr\,,\quad F_{ss}\left(\equiv \int \tau \cdot dA\right) = \int\int \tau\alpha^*(r,\theta)\cdot r d\theta dr \tag{9}$$

where p_c denotes the plastic flow pressure and τ the shearing strength.

2.3 Bearing Position

The force and moment equilibrium equations are as follows:

$$\left.\begin{aligned} &-m\ddot{h}_0 + F_{pi} + F_{OIL} + F_{sc} - F_s - F_{po} = 0 \\ &-I_x\ddot{\psi}_x + \iint p(r,\theta)\cdot r\sin\theta\cdot r dr d\theta + \iint \alpha^*(r,\theta)\cdot p_c \cdot r\sin\theta\cdot r dr d\theta - L_{piv}\cdot F_f \sin\Theta = 0 \\ &-I_y\ddot{\psi}_y - \iint p(r,\theta)\cdot r\cos\theta\cdot r dr d\theta - \iint \alpha^*(r,\theta)\cdot p_c \cdot r\cos\theta\cdot r dr d\theta + L_{piv}\cdot F_f \cos\Theta = 0 \end{aligned}\right\} \tag{10}$$

and include: the oil film shear force F_{vs}; the solid shear force F_{ss} applied to the rigid body thrust plate; the solid contact force F_{sc}; the oil film force F_{OIL}; the spring thrust force F_s; the vertical equilibrium between forces F_{po} and F_{pi} due to gas pressures inside and outside the bearing; and the moments around the pivot bearing.

The bearing model formulated here assumes complete axisymmetry, and therefore the moments around the z-axis become zero. Consequently, it is not necessary to consider the motion equation around the z-axis. From the equilibrium equations above (Equation 10), the bearing position including the bearing clearance height h_0, inclination angles (ψ_x, ψ_y) can be determined.

2.4 Procedure for Computing Numerical Values

Figure 3 shows a flow chart of the theoretical analysis of thrust slide bearing lubrication. In the figure, the dashed line shows the computation made including soft EHL. Initially, the bearing position, including bearing clearance height and gradient ψ_x, ψ_y, is assumed. Based on the assumption, the average Reynolds equation of Patir & Cheng (1978 ; 1979), Equation (2), is solved by the finite difference method (24 grid lines in the radial direction and 120 grid lines in the circumferential direction), and find the oil film force F_{OIL} from Equation (5), and the oil film viscous resistance force F_{vs} from Equation (6) are calculated. At the same time, from Equation (9), the solid contact force F_{sc} and solid frictional force F_{ss}, are found. In the event that elastic deformation is taken into account, FEM-analysis of the elastic deformation of the fixed scroll thrust plate by the oil film

pressure is undertaken. Using the FEM deformation, the oil film height distribution and the oil film pressure are computed iteratively until they converge. Finally, the bearing position is then iteratively calculated until the bearing position satisfies Equation (10) and converges.

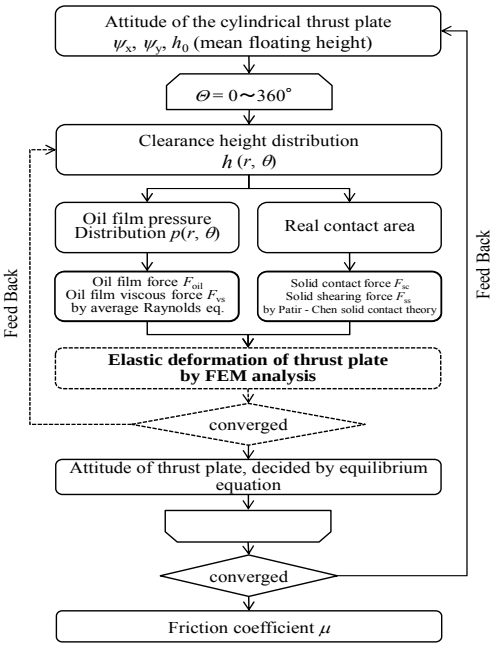

Figure 3 : Computation procedure for lubrication and attitude of thrust slide-bearing, without and with EHL pocket (dashed lines to be added for the case with EHL pocket)

Table 1 : Major specifications for computations for rigid thrust slide-bearing

Surface roughness R_a	Orbiting thrust plate [μm]	3.0
	Cylindrical thrust plate [μm]	0.056(in) ~ 0.27(out)
Standard deviation of surface roughness	Orbiting thrust plate σ_1 [μm]	1.458
	Cylindrical thrust plate σ_2 [μm]	0.188(in) ~ 1.15(out)
Bearing dimension	Outer radius r_o [mm]	65.0
	Inner radius r_i [mm]	37.85
	Friction surface area S_f [mm^2]	8772.5
Wedge angle α [mdeg]		2.92
Oil film thickness h_0 [mm]		~ 4.64 ~
Thrust plate thickness T_{th} [mm]		10.4
Pivot height L_{piv} [mm]		15.0
Cylindrical thrust plate mass m [kg]		0.340
Moment of inertia I_x, I_y [kg·m^2]		3.55×10^{-4}
Plastic flow pressure p_c [MPa]		1600
Shearing strength τ [MPa]		240
Surface density of asperities η [mm^{-2}]		400
Asperity summits radius β [μm]		8.0
Oil viscosity μ^* [Pa·s]		0.00702
Tenperature at the surface of thrust plate [°C]		70.0
Inner pressure p_{in} [Mpa]		1.0 ~ 0.8 ~ 0.5
Outer pressure p_{out} [MPa]		1.1
Pressure difference Δp [MPa]		0.1 ~ 0.3 ~ 0.6
Nominal gas thrust force F_p [kN]		~ 11.0 ~
Spring thrust force F_s [N]		600
Resultant thrust force F_T [kN]		~ 11.6 ~
Orbiting speed N [rpm]		3600
Orbiting radius r_{orb} [mm]		3.0
Sliding velocity V [m/s]		1.13
Number of grids	Radial	24
	Circumferential	120
Young modulus E [GPa]		73.5

3. ENVELOPMENT OF LUBRICATING OIL BY ELASTIC DEFORMATION OF THRUST PLATE

Numerical computation of the oil-film pressure distribution of the annular solid body model neglecting the EHL effect was undertaken by omitting the dashed line portion of the flow chart shown in Figure 3. Figure 4 shows the resulting oil pressure distribution for the model specifications given in Table 1. These specifications correspond a small scroll compressor with the motor shaft input of 0.1 kW. The annular rigid body model had the same area as that of the thrust bearing shown in the top of Figure 4(a). The inner and the outer radii were r_i = 37.85 mm and r_o = 65 mm, respectively. A pressure difference of Δp = 0.3 MPa, net downward, was applied across the bearing (between inside and the outside of bearing). In addition, an axial load of F_s = 600 N was applied to the pivot bearing section. The sum of thrust loads F_p was 11.0 kN. A mean wedge angle of α = 2.92 mdeg for one full rotation was generated on the outer circumference section of the thrust plate by this thrust load based on our FEM analysis of the thrust slide bearing. Subsequently, this wedge angle was used for the outer circumference of the annular rigid body mode. The viscosity coefficient μ^* was assumed to be 0.0081 Pa-S with an average temperature of 67.8ºC and average pressure of 0.8 MPa.

With the bottom thrust plate orbiting at a radius of r_{obt} = 3.0 mm and at a rotational speed of N = 3600 rpm, the computed oil-film pressure shown by the contour plot in Figure 4(a) was generated by the wedge effect and the squeeze effect, on the friction surface of thrust slide bearing. This oil-film pressure corresponds to the orbiting scroll thrust plate (bottom plate) moving to the left, that is, in the negative x-direction. Pressure increases from the blue color to the red color. The oil film thickness was 5.3 μm on average and 4.6 μm at minimum. The oil film pressure reaches a maximum along on the x-axis. Figure 4(b) shows the radial distribution of the oil film pressure in terms of the dimensionless radial position. In this plot, the inner circumferential position is zero and the outer circumferential position is 1.0. The oil film pressure distribution is convex upwards with a maximum value of 1.67 MPa at the front section (right side) where the radial position was 0.46 and 188 MPa on the rear section (left side) where the radial position was 0.40. Figure 4(c) shows the circumferential distribution of the maximum oil film pressure in which the angular position is measured

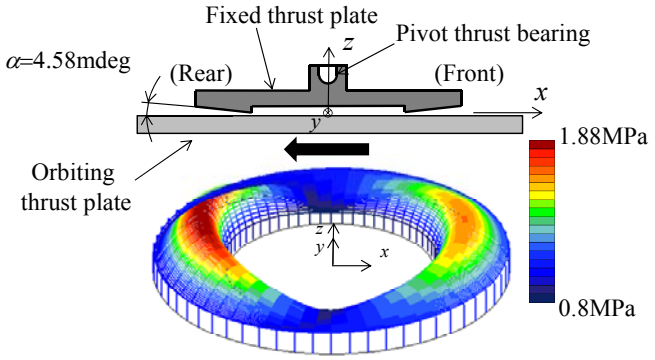

(a) Oil film pressure distribution, represented by color display.

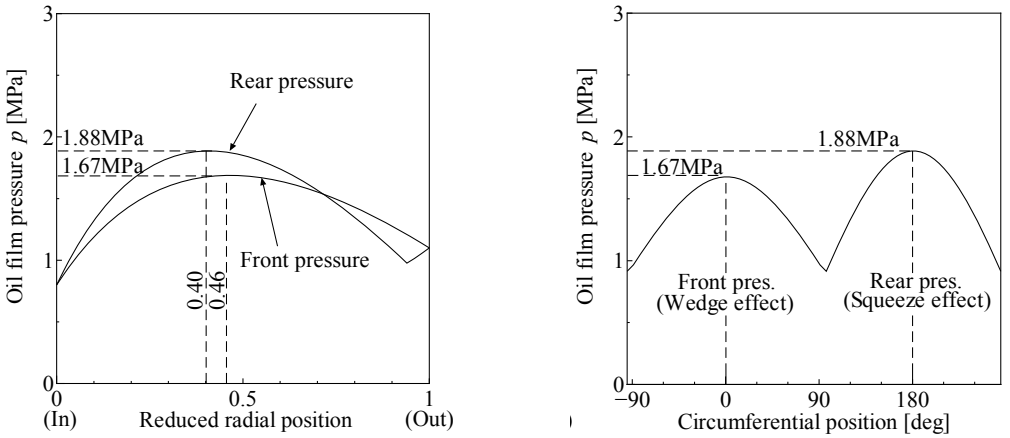

(b) Radial distribution of maximum (c) Circumferential distribution of maximum pressure

Figure 4 : Oil film pressure distribution for α=2.92 mdeg due to wedge and squeeze effects, without EHL effect.

counterclockwise from the x-axis. The oil film pressure on both the front and rear sections reaches a maximum at 0 degrees and +180 degrees (on the x-axis), respectively. The maximum pressure was greater on the rear section. The pressure at the front section, although somewhat smaller occurs at a greater radial distance where its contribution to the moment is greater. The pressure on the front section was primarily generated by the wedge effect, while that on the rear section primarily generated by the squeeze effect.

Since this large oil-film pressure was upwards convex along both the radial and circumferential directions, it was naturally assumed that the thrust plate would also be elastically deformed into an upward convex shape with this large oil film pressure. Figure 5 illustrates the elastic deformation. Since the thrust plate was loaded downward by the large gas force, the upwards convex elastic deformation tapered off at smaller radii. As expected, the elastic deformation also tapered off in the circumferential direction. This spatial deformation of the frictional surface is referred to as a pocket-shaped region in this paper. As this pocket-shaped region formed, lubricating oil particles were raked into this space as the lower thrust plate moved in the negative x-axis direction and the oil envelopment by the pocket was generated. In this manner, an even greater oil film pressure was generated. As a result, it was expected that an even better lubricating performance would be achieved at the thrust slide bearing section. This phenomenon is called “the EHL effect by lubricating oil envelopment” in this paper.

The elastic deformation of thrust plate will be verified both computationally and experimentally in the following section.

4. FEM ANALYSIS AND EXPERIMENTAL VERIFICATION OF EHL POCKET FORMATION

The pocket-shaped region generated on the frictional surface by elastic deformation of the thrust plateis called the EHL pocket in this paper. The elastic deformation of the thrust plate can be validated by FEM analysis. The analysis software, PTC Pro/ENGINEER Wildfire 5.0(on a Dell DIMENSION 8300; CPU: Core2duo, 6 shows the annular thrust plate along with the computed deformation. Figure 6(a) shows the

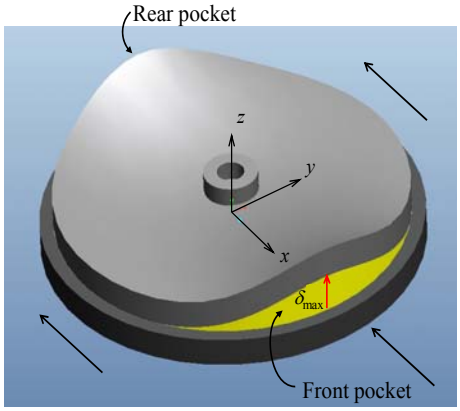

Figure 5 : Additional elastic deformation of thrust plate due to high oil-film pressure, making EHL pocket.

cross-sectional view of the thrust plate. It is not completely axisymmetric and has a rotation preventing pin, pressure guide hole, and other details that were included in the FEM model. The thrust plate is 10.4 mm thick, the inner radius of the bearing is 37.85 mm, and the outer radius is 65 mm. Inside, a 1.25 mm clearance is provided. The top center pivot bearing is modeled as well. The thrust plate material is an aluminum alloy with a Young's modulus of 73.5 GPa.

In the FEM model, the sliding surface was divided into 100 elements in the radial direction, 120 elements in the circumferential direction, and 3 elements in the thickness direction. The remaining components were meshed by the automatic element division function of the FEM software using tetrahedral solid elements. At the pivot bearing

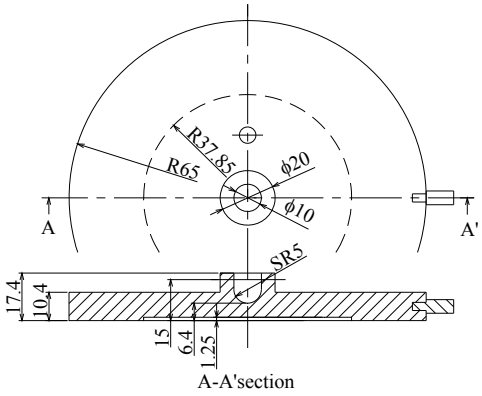

(a) Cross-sectional view of thrust plate

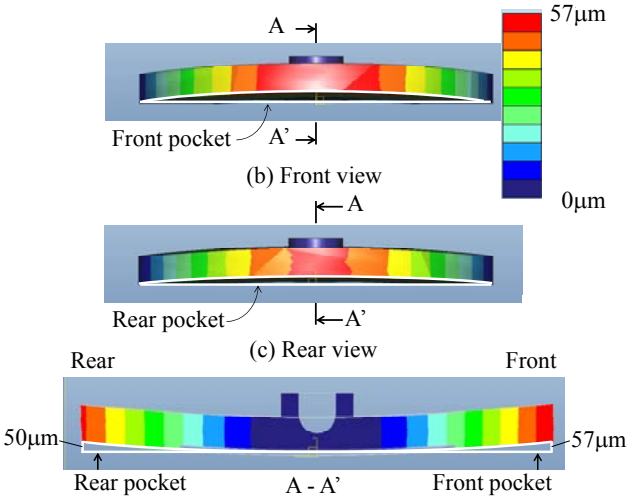

(d) A-A' cross-sectional view

Figure 6 : Thrust plate and its deformation, simulated by FEM analysis

located at the center of thrust plate, the moment was free and movements in the right/left and up/down directions were constrained. Furthermore, 1.1 MPa of pressure was applied to the outside of the bearing, and 0.8 MPa of pressure to the inside. Thus, pressure difference was 0.3 MPa; the thrust gas force due to the pressure difference was 11.0 kN The oil film pressure shown in Figure 4 was applied to the frictional surface (lower side of the thrust plate) under these conditions.

Figure 6(b) and (c) show the elastic deformation on the front and rear faces of the thrust plate. The deformation increases as the color changes from blue to red. In both views, an upwards-convex deformation was found, with no deformation along the two sides. Consequently, the frictional surface became tapered in the circumferential direction. Figure 6(d) shows section A-A'. Both front and rear surfaces (appearing as the right and left side in Figure 6(d)) were lifted and deformation was maximal on the outer circumferential portion of the clearance. Consequently, the frictional surface became tapered toward the inner circumference, too. The FEM analysis identified the pocket-shaped regions formed at both the front and the rear of the thrust bearing surface (lower side of the thrust plate) by the oil film pressure, as was postulated in the preceding section.

The biggest displacement of the outer circumferential portion of the thrust plate was 57 μm at the front section and 50 μm at the rear section. The thrust plate was substantially deformed by the oil film pressure, but the analysis assumed the oil film pressure remained constant even as the displacement increased. In reality, as the pocket size increases, the oil film pressure decreases. Consequently, the elastic deformation would be correspondingly smaller as the oil film pressure and elastic deformation to converge to an appropriate condition where the oil film pressure and elastic deformation would be balanced.

In order to validate further the pocket formation identified in the FEM analysis, friction experiments were conducted in an R-22 atmosphere. The upper portion of Figure 7 shows the set-up for the friction experiments.

The pivot bearing section of the fixed thrust plate (inner radius: 37.85 mm; outer radius: 65 mm) was held by a shaft; however, the moment is not constrained. A swing stopper is attached to the thrust plate, shown in the right-most portion of Figure 7. The lower-side thrust plate was allowed to undergo orbiting motion. The entire thrust slide bearing was immersed in an oil tank and housed inside a pressure vessel in an R-22 atmosphere pressurized to 1.1 MPa. The internal portion of the thrust slide bearing was depressurized to 0.5 MPa. Consequently, the external/internal pressure of the bearing was Δp = 0.6 MPa. The lower-side thrust plate underwent orbital motion at N = 3600 rpm.

In order to detect the drag direction of the friction force on the thrust plate, a strain gauges [1] were mounted to both sides (on the x-axis) of the shaft. The waveforms in the upper row of Figure 7(a) and (b) are the outputs from of the strain gauges. The elapsed time is along the abscissa. The strain was converted into the friction force working on the friction surface using calibration data and is plotted as the ordinate. At the instant when the friction force reaches a positive peak, the lower orbiting scroll thrust plate moves in the negative x- direction. The maximum friction force was about 50 N.

In order to detect elastic deformation due to changes in the oil film pressure acting on the thrust plate, a strain gauge [3] was mounted on the upper right surface of the fixed scroll thrust plate along the x-axis. In addition, strain gauges [2] and [4] were similarly mounted, but displaced ±45 degrees relative to the x-axis. The photograph of Figure 7 shows how they were mounted. The relevant radial positions were the center of thrust bearing section. The active gauge direction was the circumferential direction. For an assumed upwards-convex elastic deformation in the circumferential direction, these strain gauges would detect a tensile strain at their maximum sensitivity. To more easily identify pocket formation, the thrust plate thickness was reduced sequentially to 7 mm and then 5 mm, and the experiments were conducted. Since the oil-film pressure distribution shape was not changed, even with reduced plate thickness, the deformation shape appeared in a manner consistent with the FEM analysis results. The lower rows of Figure 7(a) and (b) show the measurements of elastic deformation. The strain was converted to the pocket opening height δ, as was shown in Figure 5, using by calibration data, and δ is plotted as the ordinate.

The typical height of elastic deformation δ indicated a peak precisely synchronized with the friction force. This variation of δ did not arise from the frictional force. Even if the 50 N-friction-force worked on the surface below the thrust plate, the effect could be scarcely sensed as the strain orthogonal to the frictional force in the

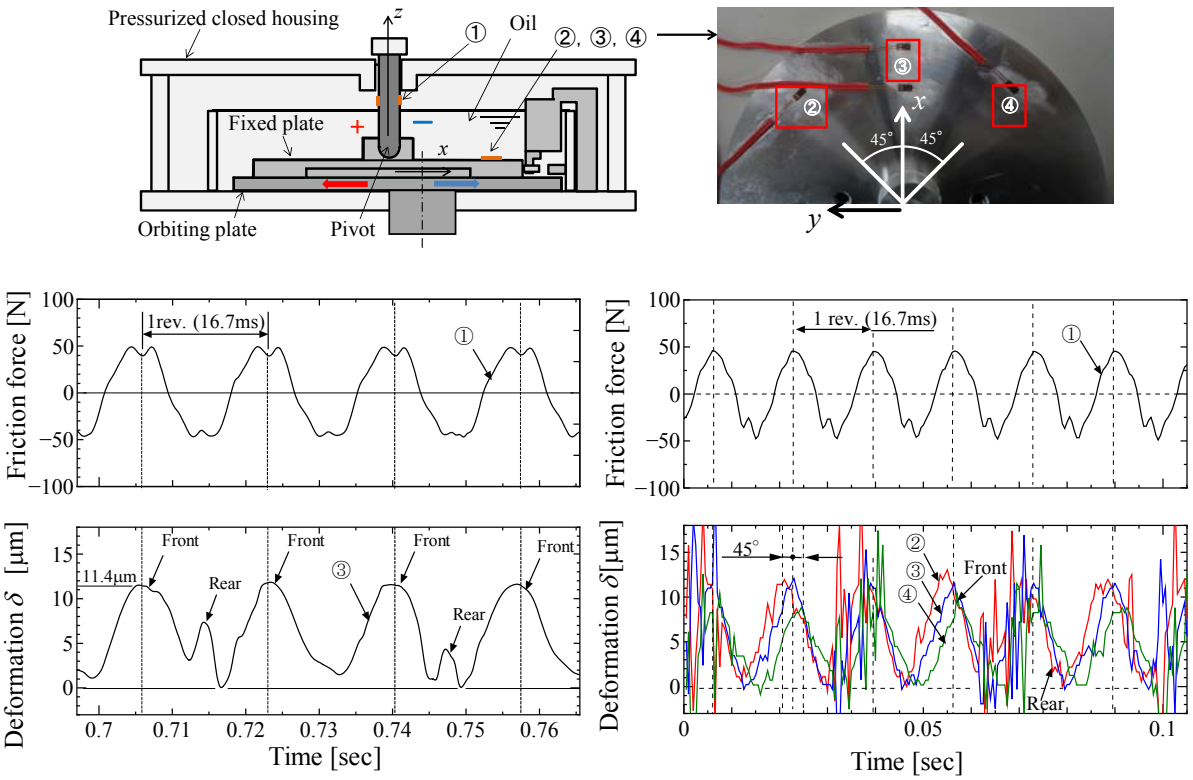

(a) Thrust plate thickness of 7 mm (b) Thrust plate thickness of 5 mm

Figure 7 : Measured dynamic deformation of the thrust plate, operated at 3600 rpm and Δp = 0.6 MPa.

circumferential direction on the top surface of thrust plate. This observation was confirmed using the FEM analysis, which predicted a circumferential strain due to the 50 N frictional force of about 0.8 με for a thrust plate thickness t = 5.0 mm. The 0.8 με was only about 1.3% of the strain rate generated by the oil film force. Other forces exerted on the thrust plate included the gas pressure and axial load by spring force, but these were held constant and did not cause variations in strain. At the same time, even if the axial load was varied, it would not result in tensile strain in the circumferential direction on the top surface of thrust plate, rather a microscopic compression strain would be generated. The compression strain would amount to only about 0.1% of the strain rate generated by the oil film force even if the axial load was assumed to vary by 0.1%. Consequently, the axial load was unconnected to variations of δ.

Among other factors that might be assumed to give rise to the elastic deformation δ, one might consider the force due to oil film pressure, shown in Figure 4, generated on the frictional surface. When δ reaches its peak, the lower orbiting scroll thrust plate moves to the left (negative x axis), and therefore, the front portion of the orbiting plate is directly beneath the location of strain gauge [3]. Since a wedge oil film pressure of up to 3 MPa was generated at the front portion of the plate, it would be appropriate to suggest that the thrust plate would undergo elastic deformation in the upward direction. The maximum typical height δ was about 11 μm when the thrust plate was 7 mm thick (Figure 7(a)). Obviously, as the thrust plate orbited, the wedge oil film pressure rotated over friction surface, and therefore, the oil film pressure right below the strain gauge gradually decreased and the measured height δ decreased accordingly. This result suggests that the thrust plate underwent upwards-convex deformation in the circumferential direction as shown in Figure 5 and Figure 6 when the deformed shape at certain times in the rotation cycle.

Near the negative peak in the friction force, that is, near where the orbiting scroll thrust plate was moving in the right (x-axis), another increase in the deformation height δ was again observed. At this time, the rear section was located directly beneath the strain gauge and a large squeeze oil film pressure (Figure 4) was generated. This variation, assume to be generated by the large squeeze oil film pressure failed to appear in the following cycle, but then re-appeared in the subsequent cycle. The variation tended to appear once every two rotations and its amplitude was small, as well. Since the squeeze pressure was expected to decrease due to elastic deformation, it was assumed that the squeeze pressure might have given rise to this kind of unstable variation. Figure 7(b) shows the experimental results when the thrust plate thickness was further reduced to 5 mm. At the rear section, severe chattering was produced. Although we cannot make any definitive statement at the present stage, one might assume that when the plate thickness was reduced, the plate was more easily bent, and the elastic deformation and the squeeze pressure were both strong and in opposite phase, resulting in severe chattering. This figure shows that the outputs of the strain gauges [2] and [4] at ±45 degrees also exhibited similar chattering. The obvious phase difference of elastic deformation output that appeared on the front section was 45 degrees, consistent with the offset angle at which the strain gauges were mounted, indicating that the pocket formed at the front section was synchronized with the orbiting motion.

5. CONCLUSION

Studies were made by experiment and theoretical analysis on the possibility of superb lubrication characteristics brought about by an EHL pocket which is formed by a thrust plate that locally undergoes elastic deformation by large oil film pressure generated in the thrust slide bearing section of a scroll compressor. The studies conducted using thrust plates of dimensions appropriate for a small-size scroll compressor with a motor shaft output of 0.1 kW. The results are summarized as follows:

(1) FEM analysis was undertaken to investigate the elastic deformation of the thrust plate by the oil film pressure; it was confirmed that a pocket-shaped region was formed.

(2) In an R-22 atmosphere, friction experiments were conducted which confirmed large elastic deformation in the front section of the thrust plate due to wedge oil film pressure; the position rotated in synchronism with the orbiting movement. In addition, the rear section was observed to undergo smaller elastic deformation relative to that of the front section which was generated once every two orbiting rotations and severe chattering occurred when the thrust plate was thin.

Discussion of the oil film pressure increase due to the oil envelopment are considered in our companion paper, Ishii, *et al.* (2014), where further studies on the EHL effect, including the calculation of the coefficient of friction in the thrust slide-bearing with and without EHL oil envelopment is presented.

NOMENCLATURE

dA : Local real contact area, m^2
F_f : Resultant frictional force, N
F_{OIL} : Oil film force, N
F_p : Nominal gas thrust force, N
F_{pi}, F_{po}: Inner gas thrust force, N
F_s : Axial spring force, N
F_{sc} : Solid contact force, N
F_{ss} : Solid shearing force, N
F_{vs} : Oil viscous force, N
h : Nominal oil film thickness, m
h_0 : Average clearance height, m
h_{ref} : Arbitrary standard thickness, m
H_r : Oil film thickness to surface roughness ratio, -
$\bar{h}_T$: Average oil film thickness, m
N : Orbital speed, rpm
p : Oil film pressure, Pa
p_a : Atmospheric pressure, Pa
p_c : Plastic flow pressure, Pa
p_{in}, p_{out} : boundary pressure, Pa
r_i, r_o : Inner bearing radius, m
$\bar{U}$, $\bar{W}$: Non-dimensional average oil flow velocity, -
$\bar{u}$, $\bar{w}$: Average oil flow velocity, m/s
U_1, V, W_1 : Boundary velocity, m/s
V_{r1}, V_{r2} : Variance ratio, -
α : Wedge angle, rad
α^* : Local solid contact ratio, -
β : Asperity summits radius, m
Δp : Pressure difference, Pa
η : Surface density of asperities, m^{-2}
Θ : Orbiting angle, rad
λ : Bearing number, -
λ^* : Non-dimensional factor for oil flow velocity, -
μ_{th} : Coefficient of friction, -
μ^* : Oil viscosity, $\mathrm{Pa \cdot s}$
σ, σ_1, σ_2: Standard deviations of surface combined roughness, m
$\bar{\sigma}$: Non-dimensional deviations of surface combined roughness, -
σ_s : Squeeze number, -
τ_t : Non-dimensional time, rad
τ : Shearing strength, Pa
ϕ : Pressure flow factor, -
ϕ_s : Shear flow factor, -
ϕ_f, ϕ_{fs} : Shear stress factor, -
ψ_x, ψ_y : Rotation angle rotating x - axis, rad
ω : Angular orbiting velocity, rad/s

REFERENCES

Greenwood, J. A., Williamson, J. B. P., 1966 , "Contact of nominally flat surfaces", *Proceeding of Royal Society of London*, A Vol. 295 : p. 300-319.

Ishii, N., Oku, T., Anami, K., Knisely, C. W., Sawai, K., Morimoto, T., Iida, N., 2008, "Experimental Study of the Lubrication Mechanism for Thrust Slide Bearings in Scroll Compressors", *An International Journal of Heating, Air-Conditioning and Refrigerating Research (HVAC&R Research)*, *ASHRAE*, Vol. 14, No. 3: p. 453 - 465.

Ishii, N., Tsuji, T., Anami, K., Nokiyama, K., Yoshida, H., Nakai, H., Oku, T., Sawai, K., Knisely, C.W., 2014, "Optimization of EHL Performance in Thrust Slide-Bearing of Scroll Compressors," submitted to 2014 Purdue Herrick Conferences.

Oku, T., Ishii, N., Anami, K., Knisely, C. W., Sawai, K., Morimoto, T., Hiwata, A., 2008, "Theoretical Model of Lubrication Mechanism in the Thrust Slide-Bearing of Scroll Compressors", *An International Journal of Heating, Air-Conditioning and Refrigerating Research (HVAC&R Research)*, *ASHRAE*, Vol. 14, No. 2 : p. 239-358.

Patir, N. and Cheng, H. S., 1978, "An average flow model for determining effects of three - dimensional roughness on partial hydrodynamic lubrication", *Transaction of the ASME*, Journal of Lubrication Technology, Vol. 100, No. 1 : p. 12-17.

Patir, N. and Cheng, H. S., 1979, "Application of average flow model to lubrication between rough sliding surfaces", Transaction of the ASME, *Transaction of the ASME*, Journal of Lubrication Technology, Vol. 101, No. 2 : p. 200-229.

Tsuji, T., 2014, "A Study of Refrigerant Compressors for Higher Performance, Part 1: Design Guideline for Performance Optimization of Reciprocating Compressors; Part 2: Oil Envelopment Phenomenon in Thrust Slide-Bearing of Scroll Compressors and Soft EHL Analysis," *Doctoral Thesis*, presented to Osaka Electro-Communication University.

ACKNOWLEDGMENT

The authors wish to thank Professor Hiroshi Yabe at Osaka Electro-Communication University, Mr. Shuichi Yamamoto, Senior Councilor, R&D Division, Panasonic Co., Ltd., Mr. Kiyoshi Imai, Vice President, Corporate Engineering Division, Appliances Company, Panasonic Corporation, and Mr. Masahiro Atarashi, Director, Appliances Company, Panasonic Corporation for their encouragement and valuable assistance in carrying out this work and their permission to publish this study.